Three-dimensional Contact Analysis of Human Wrist Joint using MRI

Keisuke SASAGAWA[1], Makoto SAKAMOTO[2], Hidenori YOSHIDA[2], Koichi KOBAYASHI[2] and Yuji TANABE[3]

[1]Venture Business Laboratory, Niigata University, Niigata 950-2181, Japan
[2]Department of Health Sciences, Niigata University School of Medicine, Niigata, Japan
[3]Department of Mechanical and Production Engineering, Niigata University, Niigata, Japan

Abstract

The wrist is a complex joint, consisting of the eight small carpal bones that articulate with each other, the metacarpals distally, and the radius, ulna, and triangular fibrocartilage complex proximally. The wrist joint carries out complicated motions that combine palmar/dorsal flexion with radio/ulnar deviation. Knowledge of in vivo joint mechanics is important for understanding pathological mechanisms and the treatment of various joint problems. To examine wrist joint contact mechanisms, in vitro cadaveric studies have been performed using pressure-sensitive film. Investigations on in vivo joint contact mechanisms for wrist motion have rarely been reported. The aim of this study is to investigate in vivo wrist joint contact mechanisms during palmar/dorsal flexion by magnetic resonance imaging (MRI). Magnetic Resonance scanning was performed on the left wrist of twelve participants using a 1.5T-MRI system (Achieva, Philips Medical Systems, Best, Netherlands). The wrist joint was scanned at 5 positions (palmar flexion, –30 degree; neutral, 0 degree; and dorsal flexion, 30, 60 and 90 degrees). Quantitative analysis of wrist joint contact mechanisms was performed for 12 normal radioscaphoid and radiolunate joints. The in-plane motions of the scaphoid and lunate were measured. The contact area at the radioscaphoid joint was significantly greater than that at the radiolunate joint in all wrist positions. The contact area increased with increasing wrist angle, and the contact distributions indicated by 3–D models of the scaphoid and lunate were moved during palmar/dorsal flexion. Contributions of the scaphoid and lunate to in-plane motion at 60 degrees of dorsal flexion were 74% and 52%, respectively.

1. Introduction

The wrist is a complex joint consisting of eight small carpal bones. These carpi are divided into two rows: the distal row consisting of the trapezium, trapezoid, capitate, and hamate; and the proximal row consisting of the scaphoid, lunate, triquetrum, and pisiform. The bones in these two rows are articulated with each other. The wrist joint comprises the radiocarpal joint, which includes the radioscaphoid and radiolunate joints. The radioscaphoid joint consists of the scaphoid and radius, and the radiolunate joint consists of the lunate and radius. The radiocarpal joint is condyloid and capable of movement through two axes: palmar/dorsal flexion (flexion/extension) and radial/ulnar deviation. The wrist joint carries out complicated motions that combine

palmar/dorsal flexion with radio/ulnar deviation. The anatomy of the wrist joint is shown in Fig.1.

Knowledge of in vivo joint mechanics is important for understanding the pathological mechanisms and the treatment of various joint problems. Kienböck's disease that is one of wrist diseases is known as osteonecrosis of the lunate; its cause remains unknown. It is pointed out that Kienböck's disease is related to pressure on the lunate [1]. During a fall to the ground, the wrist in the extended position is subjected to extremely high compressive loads, often resulting in fracture of the distal radius or scaphoid; however, the pathoanatomy remains unclear [2]. To examine the wrist joint contact mechanics, in vitro cadaveric studies have been performed using various techniques [3-7]. Pressure-sensitive film allowed investigators to measure the pressure distribution, contact area, and contact force [5, 6]; and thin-film electronic pressure sensors have enabled dynamic measurement of pressure distribution [7]. However, these techniques are employed only in cadaveric studies. On the other hand,
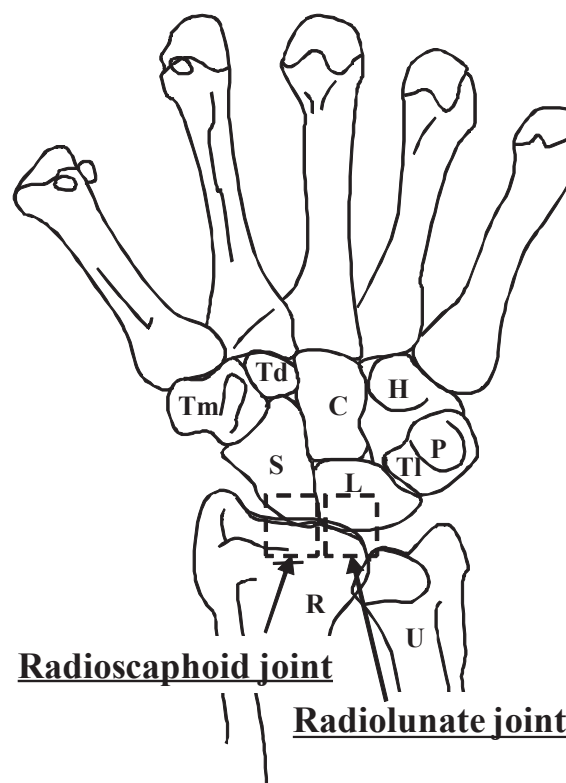

Fig.1 Structure of wrist joint. Each bone is expressed by the abbreviation; R: radius, U: ulna, S: scaphoid, L: lunate, Tl: triquetral, P: pisiform, Tm: trapezium, Td: trapezoid, C: capitate, H: hamate. The radioscaphoid and radiolunate joints are shown by broken lines

many theoretical studies have been performed for analysis of wrist joint pressure distribution [8-13]. The in vivo study is essential to understand normal joint mechanism in detail. Recently, for in vivo studies of human joint contact mechanisms, magnetic resonance imaging (MRI) to visualize articular cartilage has attracted attention. The patellofemoral joint contact mechanism has been examined in vivo by MRI [14, 15] and it was reported that MRI was an effective method for examining joint contact in vivo.

Investigations of in vivo contact mechanisms for the wrist joint have been reported less frequently than those for the other joints such as the knee joint, and in vivo joint contact distribution during wrist motion is still unknown. The purpose of this study was to investigate the in vivo joint contact mechanism during wrist motion by MRI. The joint contact during palmar/dorsal flexion (flexion/extension) was estimated from derived MR images. We performed a quantitative three-dimensional (3-D) analysis of the human wrist contact area distribution, and measured the motions of the scaphoid and lunate during palmar/dorsal flexion.

2. Materials and Methods
2.1 Image acquisition
Twelve human participants (mean age 23.8 ± 2.5 years, nine male, three female) who had no history of bone and joint diseases were enrolled in this study. Their left wrists were scanned using a 1.5-T MRI system (Achieva, Philips Medical Systems, Netherlands) with a surface coil. A principle of selective excitation technique sequence was used so that cartilage was visualized clearly (TR = 20 msec, TE = 8.2 msec, Flip angle = 25 degrees). The wrist joint was scanned at 5 positions (–30 degrees of palmar flexion, neutral, and 30, 60, and 90 degrees of dorsal flexion) during palmar/dorsal flexion (Fig.2). The home-made devices were used to hold the wrist position. These devices avoid the movement of the wrist during MR scanning, and have no effect on MR scan. The wrist images were acquired in the coronal plane. The field of view (FOV) was 100 mm with a matrix of 512 × 512. The slice thickness was 0.5 mm. The scanning time was about six minutes.

2.2 Joint contact analysis
Joint contact area was determined by measuring the length of visible contact between the radius and scaphoid, and the radius and lunate in each slice (Fig.3), multiplying this length by the slice thickness (0.5 mm), and then summing these values to obtain the total contact area (mm^2) [16]. This method is highly reproducible and comparable to established pressure-sensitive film techniques [17]. A single examiner performed all the contact area measurements, repeating each measurement four times per scan, to obtain an average contact area for each wrist position and condition.

2.3 Reconstruction of three-dimensional surface models
The 3-D surface models of the scaphoid, lunate, and radius, including cartilage surface data, were reconstructed from MR image sets with a commercial software package
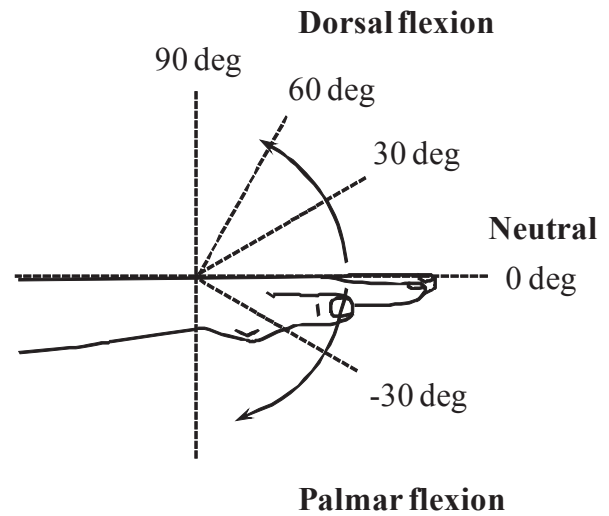

Fig.2 Scanning position of the wrist joint. A neutral position of the wrist is defined as zero. Positive and negative angle values express dorsal and palmar flexion, respectively

Fig.3 Typical coronal MR image used for calculating contact area. R: radius, S: scaphoid, L: lunate

(ZedView DB 4.0, Lexi, Japan). Segmentation of bone and cartilage regions was performed manually. 3-D surface models of bone with cartilage were used in the creation of joint contact distribution maps and the motion analysis of the scaphoid and lunate.

2.4 Motion analysis
Kinematics of the scaphoid and lunate were analyzed by each 3-D bone surface model. The positions of the scaphoid and lunate at all wrist angles were studied. For the radiocarpal joint in a sagittal view, the in-plane motion of the scaphoid and lunate during palmar/dorsal flexion was examined by comparing with the positions of bones at neutral. The position of the scaphoid was determined by the long shaft of the scaphoid. The position of the lunate was determined by the line connecting the distal edges of dorsal and palmar side.

3. Results

The 3-D model of the radiocarpal joint in a sagittal view is shown in Fig.4(a). At −30 degrees of palmar flexion, the position of the scaphoid which expressed by the long shaft of the scaphoid was roughly perpendicular to the long shaft of the radius. The position of the lunate which expressed by the line connecting the distal edges of dorsal and palmar side was rotated palmarly than the position of the scaphoid. During dorsal flexion, the scaphoid and lunate were rotated dorsally. At 90 degrees of dorsal flexion, the scaphoid was rotated to a position that was parallel to the radius shaft. The contact area map on the radius is shown in Fig.4(b). During from palmar flexion to dorsal flexion, the contact area on the scaphoid fossa that found in the palmar side was moved toward the dorsal side. The contact area on the lunate fossa was found in the center of the fossa in two wrist angles. The scaphoid and lunate are rotated depending on the wrist angle. The rotational changes of the scaphoid and lunate during the motion of the wrist from −30 degrees to 90 degrees were estimated (Fig.5). The scaphoid rotated more greatly than the lunate. During the wrist angle changes from −30 degrees to 90 degrees, the ranges of motion for the scaphoid and lunate were 82 degrees and 57 degrees, respectively. At 60 degrees of dorsal flexion, the rotational angles of the scaphoid and lunate were 44.5 degrees and 31.2 degrees, respectively. Then, the contributions of the scaphoid and lunate to in-plane motion at 60 degrees of dorsal flexion were 74% and 52%, respectively.

During palmar/dorsal flexion, the joint contact distribution was analyzed for twelve participants (#1 - #12). The joint contact distribution map of the scaphoid and lunate at 5 wrist positions are shown in Fig.6. In most wrist angles, the contact areas of the radioscaphoid joint were greater than those of the radiolunate joint. The radioscaphoid joint contacts were confirmed in all wrist angles examined. However, in the radiolunate joint, there was no contact at some wrist angles. Especially, the radiolunate joints for participants #2, #4, and #8 had little contact during palmar/dorsal flexion. For all participants,
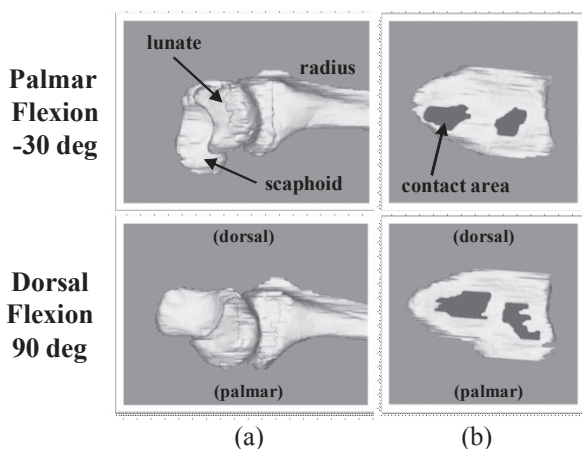
the contact area moved from the palmar side to the dorsal side during palmar/dorsal flexion. It was noted that joint contacts were dependent on individual anatomy. The joint contact area was measured directly from MR images. The average contact area in twelve participants during palmar/dorsal flexion was calculated (Fig.7). At neutral, the mean contact areas for the radioscaphoid and
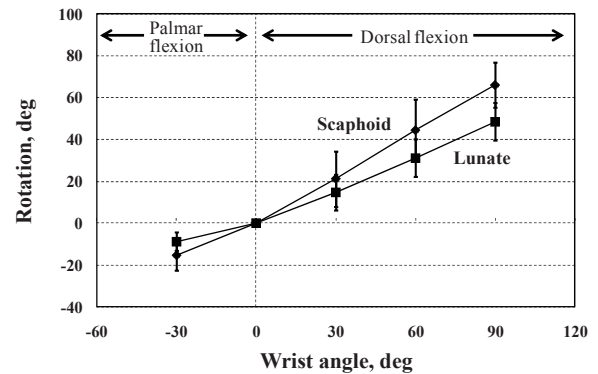

Fig.5 Rotational changes for the scaphoid and lunate during palmar/dorsal flexion. The mean and standard deviation of the rotational angles for twelve participants are shown
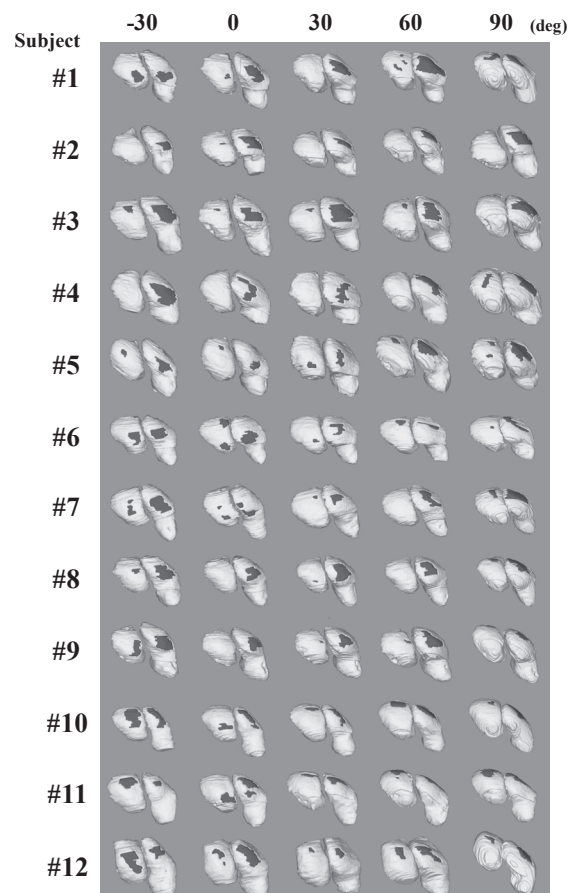

Fig.6 Contact area distribution map of radiocalpal joint. At radioscaphoid and radiolunate joint, contact distributions on a scaphoid (left) and a lunate (right) are shown. The joint contact region is shown by a dark region on each cartilage. For each bone the upper is palmar, and the lower is dorsal

Fig.4 3-D model of the radiocarpal joint at −30 degrees of palmar flexion and 90 degrees of dorsal flexion. (a) Positions of the scaphoid, lunate, and radius at sagittal view are shown. (b) Contact areas of the scaphoid fossa (left) and lunate fossa (right) on the radius are shown

radiolunate joints were 40.3 ± 13.1 mm^2 and 8.7 ± 10.0 mm^2, respectively. The radioscaphoid contact area was significantly greater than the radiolunate contact area. The radioscaphoid joint had the lowest contact area (36.6 mm^2) at 30 degrees of dorsal flexion, and the highest contact area (68.7 mm^2) at 90 degrees of dorsal flexion. The radiolunate joint had the lowest contact area (3.7 mm^2) at 30 degrees of dorsal flexion, and the highest contact area (19.9 mm^2) at –30 degrees of palmar flexion. In both the radioscaphoid and radiolunate joints, it was observed that an increase in wrist angle increased the contact area.
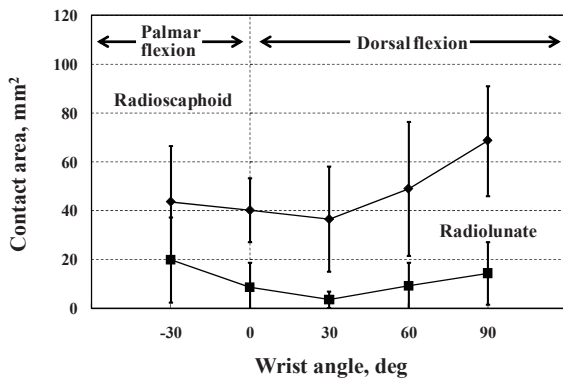

Fig.7 Changes in contact area at the radioscaphoid and radiolunate joints during palmar/dorsal flexion. The mean and standard deviation of the contact areas for twelve participants are shown

4. Discussion

MRI, like computed tomography, is an effective method for observing physical internal structures non-invasively. In particular, the MR scan is a powerful method for imaging soft tissues without radiation. However, MR scans visualize bones poorly, and the MR intensity of bone is non-uniform. Therefore, it is difficult to describe bone structure from MR images. To reconstruct 3-D bone surface models from MR image sets, the boundary between bone and soft tissue must be apparent. 3-D bone surface models can be reconstructed from the detected bone outlines. Recently, we investigated the accuracy of 3-D MRI-based bone surface models by comparison with an actual bone and reported that the surface error in the 3-D MRI-based bone model was 1.1 mm [18]. This illustrates the potential of 3-D MRI-based bone models to investigate joint mechanisms in vivo.

Until now, investigations of wrist joint contact mechanism have been performed in cadaveric studies [2-6]. To the best of our knowledge, the only in vivo study was a report of Pillai et al. [19], who evaluated in vivo contact mechanics of the wrist joint during light grasping. These data from the literature on radioscaphoid and radiolunate contact areas for the neutral position are summarized in Table 1. Viegas et al. [3] and Tencer et al. [4] investigated the ratio of the contact areas in the radioscaphoid to radiolunate using a cadaver wrist and pressure-sensitive film, and these ratios were 0.26 and 0.27, respectively. Pillai et al. [19] reported that the values of the contact areas of the radioscaphoid and radiolunate joints were 41.6 mm^2 and 10.2 mm^2, respectively. Our results for the radioscaphoid and radiolunate contact areas were almost consistent with those of Pillai et al. [19]. The ratio of the radiolunate to radioscaphoid contact areas for all wrist angles ranged from 0 to 3.37. It is thought that the contact mechanism of the radioscaphoid joint is different from that of the radiolunate joint. It will be necessary to carry out further in vivo investigations into the contact mechanism for the radioscaphoid and radiolunate joints during radial/ulnar deviation.

Change of the joint contact distribution is closely connected with the motion of carpal bones. Contributions of the scaphoid and lunate to in-plane motion at 60 degrees of dorsal flexion were 74% and 52%, respectively. Moojen et al. [20] investigated the kinematics of carpal bones using CT scan. They reported that contributions of the scaphoid and lunate to 60 degrees of dorsal flexion were 87% and 66%, respectively. Wolfe et al. [21], who performed the CT kinematics analysis, concluded that 83% and 45% of global wrist dorsal flexion occurs at the radioscaphoid joint

Table 1 Contact area data of wrist joint

Author(s) (subject numbers)	Subjects	Radioscaphoid contact area (mm^2)	Radiolunate contact area (mm^2)	Radiolunate contact area / Radioscaphoid contact area	Contact area / Total joint area
Viegas et al. (1987) (n=10)	Cadaver	—	—	0.26	0.10 (S) 0.11 (L)
Tencer et al. (1988) (n=10)	Cadaver	—	—	0.27	0.21
Kazuki et al. (1991) (n=4)	Cadaver	—	—	—	0.19
Pillai et al. (2007) (n = 4)	In Vivo	41.6 ± 24.5	10.2 ± 3.9	0.24	—
Present study (n = 12)	In Vivo	40.3 ± 13.1	8.7 ± 10.0	0.22	0.19 (S) 0.04 (L)

(S): Scaphoid, (L): Lunate

and radiolunate joint, respectively. The motion of the carpal bones during wrist motion is influenced by ligament and tendon. MRI can visualize soft tissues such as articular cartilage, ligament and tendon. Therefore, the kinematics analysis that considered the soft tissue may be possible.

5. Conclusion
We investigated the in vivo joint contact mechanism of the human wrist during palmar/dorsal flexion and observed the following: (1) The contact areas on the scaphoid and lunate were markedly moved from the dorsal side to the palmar side during palmar/dorsal flexion. (2) There were wrist angles for which no radiolunate contact was found, while radioscaphoid contacts were observed at every wrist position in palmar/dorsal flexion. (3) The joint contact area was increased with increasing wrist angle during palmar/dorsal flexion. (4) The possibility of the kinematics analysis that considered the soft tissue was suggested.

References
[1] Gunal, I., Ozcan, O., Uyulgan, B., Baran, O., Arman, C. and Karatosun, V.: Biomechanical analysis of load transmission characteristics of limited carpal fusions used to treat Kienböck's disease. *Acta Orthop Traumatol Turc*, **39** (2005), 351-355.
[2] Rettig, M.E., Dassa, G.L., Raskin, K.B. and Melone, C.P. Jr.: Wrist fractures in the athlete: Distal radius and carpal fractures. *Clinics in Sports Medicine*, **17** (1998), 469-489.
[3] Viegas, S.F., Tencer, A.F., Cantrell, J., Chang, M., Clegg, P., Hicks, C., O'Meara, C. and Williamson, J.B.: Load transfer characteristics of the wrist. I: The normal joint. *Journal of Hand Surgery*, **12A** (1987), 971-978.
[4] Tencer, A.F., Viegas, S.F., Cantrell, J., Chang, M., Clegg, P., Hicks, C., O'Meara, C. and Williamson, J.B.: Pressure distribution in the wrist joint. *Journal of Orthopedic Research*, **6** (1988), 509-517.
[5] Kazuki, K., Kusunoki, M. and Shimazu, A.: Pressure distribution in the radiocarpal joint measured with a densitometer designed for pressure-sensitive film. *Journal of Hand Surgery*, **16A** (1991), 401-408.
[6] Wagner, W.F., Tencer, A.F., Kiser, P. and Trumble, T.E.: Effects of intra-articular distal radius depression on wrist joint contact characteristics. *Journal of Hand Surgery*, **21A** (1996), 554-560.
[7] Hara, T., Horii, E., An, K., Cooney, W.P., Linscheid, R.L. and Chao, E.Y.S.: Force distribution across wrist joint: application of pressure-sensitive conductive rubber. *Journal of Hand Surgery*, **17A** (1992), 339-347.
[8] Horii, E., Garcia-Elias, M., An, K.N., Bishop, A.T., Cooney, W.P., Linscheid R.L. and Chao E.Y.: Effect on force transmission across the carpus in procedures used to treat Kienböck's disease. *Journal of Hand Surgery*, **15A** (1990), 393-400.
[9] Chuind, F., Cooney, W.P., Linscheid, R.L., An, K.N. and Chao, E.Y.: Force and pressure transmission through the normal wrist. A theoretical two-dimensional study in the posteroanterior plane. *Journal of Biomechanics*, **28** (1995), 587-601.
[10] Genda, E., Horii, E., Suzuki, Y., Kasahara, T. and Tanaka, Y.: Three dimensional rigid body spring modeling and its application for human joints. *Proceeding Computer Methods in Biomechanics and Biomedical Engineering*, **6** (1998), 59-65.
[11] Genda, E. and Horii, E.: Theoretical stress analysis in wrist joint—neutral position and functional position. *Journal of Hand Surgery*, **25B** (2000), 292-295.
[12] Iwasaki, N., Genda, E., Barrance, P.J., Minami, A., Kaneda, K. and Chao, E.Y.: Biomechanical analysis of limited intercarpal fusion for the treatment of Kienbock's disease: a three−dimensional theoretical study. *Journal of Orthopedic Research*, **16** (1998), 256-263.
[13] Majima, M., Horii, E., Matsuki, H., Hirata, H. and Genda, E.: Load transmission through the wrist in the extended position. *The American Society for Surgery of the Hand*, **33A** (2008), 182-188.
[14] Besier, T.F., Gold, G.E., Beaupre, G.S. and Scott, L.: A Modeling Framework to Estimate Patellofemoral Joint Cartilage Stress In Vivo. *Medicine and Science Sports and Exercise*, **37** (2005), 1924-1930.
[15] Gold, G.E., Besier, T.F., Draper, C.E., Asakawa, D.S., Delp, S.L. and Beaupre, G.S.: Weight−bearing MRI of patellofemoral joint cartilage contact area. *Journal of Magnetic Resonance Imaging*, **20** (2004), 526-530.
[16] Brechter, J.H. and Powers, C.M.: Patellofemoral joint stress during stair ascent and descent in persons with and without patellofemoral pain. *Gait Posture*, **16** (2002), 115-23.
[17] Brechter, J.H., Powers, C.M., Terk, M.R., Ward, S.R. and Lee, T.Q.: Quantification of patellofemoral joint contact area using magnetic resonance imaging. *Magnetic Resonance Imaging*, **21** (2003), 955-959.
[18] Sasagawa, K., Watanabe, S., Kobayashi, K., Sakamoto, M., Tanabe, Y., Sato, T. and Koga, Y.: Accuracy examination of three-dimensional bone surface model using MRI and CT. *Journal of Japanese Society for Clinical Biomechanics*, **29** (2008), 397-402 (in Japanese).
[19] Pillai, R.R., Thoomukuntla, B., Ateshian, G.A. and Fischer, K.J.: MRI−based modeling for evaluation of in vivo contact mechanics in the human wrist during active light grasp. *Journal of Biomechanics*, **40** (2007), 2781-2787.
[20] Moojen, T.M., Snel, J.G., Ritt, M.J.P.F., Venema, H.W., Kauer, J.M.G. and Bos, K.E.: In vivo analysis of carpal kinematics and comparative review of the literature. *Journal of Hand Surgery*, **28A** (2003), 81-87.
[21] Wolfe, S.W., Neu, C. and Crisco, J.J.: In vivo scaphoid, lunate, and capitate kinematics in flexion and in extension. *Journal of Hand Surgery*, **25A** (2000), 860-869.